Earth and Planetary Science Letters 463 (2017) 159–170

Contents lists available at ScienceDirect

Earth and Planetary Science Letters

www.elsevier.com/locate/epsl

Perspectives on Proterozoic surface ocean redox from iodine contents in ancient and recent carbonate

Dalton S. Hardisty [a,l,*], Zunli Lu [b], Andrey Bekker [a,c], Charles W. Diamond [a], Benjamin C. Gill [d], Ganqing Jiang [e], Linda C. Kah [f], Andrew H. Knoll [g], Sean J. Loyd [h], Magdalena R. Osburn [i], Noah J. Planavsky [j], Chunjiang Wang [k], Xiaoli Zhou [b], Timothy W. Lyons [a]

[a] Department of Earth Sciences, University of California, Riverside, CA, USA
[b] Department of Earth Sciences, Syracuse University, Syracuse, NY, USA
[c] Department of Geology, University of Johannesburg, South Africa
[d] Department of Geosciences, Virginia Polytechnic and State University, Blacksburg, VA, USA
[e] Department of Geoscience, University of Nevada, Las Vegas, NV, USA
[f] Department of Earth and Planetary Sciences, University of Tennessee, Knoxville, TN, USA
[g] Department of Earth and Planetary Sciences, Harvard University, Cambridge, MA, USA
[h] Department of Geological Sciences, California State University, Fullerton, CA, USA
[i] Department of Earth and Planetary Sciences, Northwestern University, Evanston, IL, USA
[j] Department of Geology and Geophysics, Yale University, New Haven, CT, USA
[k] College of Geosciences, China University of Petroleum, Beijing, China
[l] Department of Geology and Geophysics, Woods Hole Oceanographic Institute, Woods Hole, MA, USA

ARTICLE INFO

Article history:
Received 10 September 2016
Received in revised form 23 January 2017
Accepted 25 January 2017
Available online 14 February 2017
Editor: H. Stoll

Keywords:
Proterozoic oxygen
Shuram isotope anomaly
carbonate diagenesis
Bahamas
iodine
metazoan evolution

ABSTRACT

The Proterozoic Eon hosted the emergence and initial recorded diversification of eukaryotes. Oxygen levels in the shallow marine settings critical to these events were lower than today's, although how much lower is debated. Here, we use concentrations of iodate (the oxidized iodine species) in shallow-marine limestones and dolostones to generate the first comprehensive record of Proterozoic near-surface marine redox conditions. The iodine proxy is sensitive to both local oxygen availability and the relative proximity to anoxic waters. To assess the validity of our approach, Neogene–Quaternary carbonates are used to demonstrate that diagenesis most often decreases and is unlikely to increase carbonate-iodine contents. Despite the potential for diagenetic loss, maximum Proterozoic carbonate iodine levels are elevated relative to those of the Archean, particularly during the Lomagundi and Shuram carbon isotope excursions of the Paleo- and Neoproterozoic, respectively. For the Shuram anomaly, comparisons to Neogene–Quaternary carbonates suggest that diagenesis is not responsible for the observed iodine trends. The baseline low iodine levels in Proterozoic carbonates, relative to the Phanerozoic, are linked to a shallow oxic–anoxic interface. Oxygen concentrations in surface waters would have at least intermittently been above the threshold required to support eukaryotes. However, the diagnostically low iodine data from mid-Proterozoic shallow-water carbonates, relative to those of the bracketing time intervals, are consistent with a dynamic chemocline and anoxic waters that would have episodically mixed upward and laterally into the shallow oceans. This redox instability may have challenged early eukaryotic diversification and expansion, creating an evolutionary landscape unfavorable for the emergence of animals.

1. Introduction

The shallow oceans of the Proterozoic Eon were the host to both photosynthetic oxygen production and the sequential origin and radiations of eukaryotes and animals (Knoll, 2014; Lyons et al., 2014). Nevertheless, the current conversation about the oxygenation of the biosphere, the first appearances and diversification of the earliest eukaryotes and animals, and their associated oxygen demands (Mills et al., 2014; Sperling et al., 2013) has often focused instead on conditions in the atmosphere (Planavsky et al., 2014) and sub-photic deep-marine waters (Gilleaudeau and Kah, 2015;

* Corresponding author at: Department of Geology and Geophysics, Woods Hole Oceanographic Institute, Woods Hole, MA, USA.
E-mail address: dhardisty@whoi.edu (D.S. Hardisty).

http://dx.doi.org/10.1016/j.epsl.2017.01.032
0012-821X/

Partin et al., 2013; Reinard et al., 2013; Sperling et al., 2015). Such comparisons are indirect, since *in situ* oxygenic photosynthesis in the shallow photic zone provides the potential for elevated shallow-ocean oxygen at micromolar (μM) levels even under an anoxic atmosphere (Reinhard et al., 2016). This disconnect reflects a shortage of carbonate geochemical redox proxies specific to local shallow ocean conditions. The need to fill this knowledge gap is particularly critical through the mid-Proterozoic (ca. 1.8 to 0.8 billion years ago or Ga), which precedes the evolution of the earliest metazoans (Knoll, 2014).

Geochemical proxies that track the mobilization of iron and manganese in mid-Proterozoic soils are consistent with mid-Proterozoic pO_2 as low as <0.1–1% of present atmospheric levels (PAL) (Cole et al., 2016; Crowe et al., 2013; Mitchell and Sheldon, 2009; Planavsky et al., 2014). If these estimates are correct, the predicted nanomolar (nM) to low μM equilibrium-driven levels of dissolved O_2 in the surface ocean are likely to have inhibited eukaryote diversification (Planavsky et al., 2014; Reinhard et al., 2016). Limited carbonate paleoredox proxy records (REE's, Zn/Fe) are generally consistent with low atmospheric pO_2 through portions of the Proterozoic (Liu et al., 2016; Tang et al., 2016) and extensive records of redox-sensitive metals (Mo, Cr, U, Fe) in basinal black shale specifically fingerprint an anoxic deeper ocean dominated by a combination of ferruginous and sulfidic (euxinic) waters (Gilleaudeau and Kah, 2015; Partin et al., 2013; Reinhard et al., 2013; Sperling et al., 2015).

Ratios of iodine-to-calcium-magnesium, or I/(Ca + Mg), in shallow-marine carbonates can track the presence or absence of O_2 in the shallow ocean (Hardisty et al., 2014) and the position of the oxic–anoxic interface in the water column relative to the site of carbonate precipitation (Lu et al., 2016). The oxidized and reduced iodine species, iodate (IO_3^-) and iodide (I^-), respectively, constitute the bulk of total dissolved iodine ($IO_3^- + I^-$) in seawater (Chance et al., 2014; Emerson et al., 1979; Farrenkopf and Luther III, 2002; Rue et al., 1997; Wong and Brewer, 1977). In marine waters, IO_3^- and I^- concentrations are inversely correlated, with nearly uniform vertical profiles of total dissolved iodine outside of a slight depletion in photic waters. Concentrations of total dissolved iodine in modern seawater are near 450–500 nM (Chance et al., 2014), globally uniform, and have a residence time (~300 kyrs) that is orders of magnitude longer than the mixing time of the ocean. Importantly, IO_3^- exists exclusively in oxic waters, with IO_3^- reduction occurring in weakly oxic waters prior to the onset of iron and sulfate reduction (Fig. 1; Emerson et al., 1979; Farrenkopf and Luther III, 2002; Kennedy and Elderfield, 1987a, 1987b; Rue et al., 1997; Wong and Brewer, 1977). Quantitative IO_3^- reduction is observed within anoxic basins (Emerson et al., 1979; Wong and Brewer, 1977) and in reducing pore waters (Kennedy and Elderfield, 1987a, 1987b). The redox behavior of iodine can be traced for ancient oceans because IO_3^- is the sole iodine species that co-precipitates with carbonate rocks (Lu et al., 2010). Thus, carbonate minerals formed in anoxic waters—where I^- is the predominant dissolved iodine species—are not expected to incorporate iodine during precipitation, as demonstrated in calcite synthesis experiments (Lu et al., 2010). This expectation is consistent with previous reports noting a lack of iodine in carbonate rocks prior to the Great Oxidation Event (GOE) (Hardisty et al., 2014).

Although quantitative reduction of IO_3^- occurs within hours in low-oxygen and anoxic waters (Farrenkopf et al., 1997), I^- oxidation can be a slower process, with rate estimates ranging from weeks to years (Chance et al., 2014; Luther III et al., 1995). Due to this redox asymmetry, the largest gradients in marine IO_3^- concentrations occur within the oxycline of oxygen-minimum zone (OMZs) or anoxic basins (Fig. 1; Farrenkopf and Luther III, 2002; Rue et al., 1997). In this weakly oxic zone, IO_3^- reduction becomes favorable but is not quantitative and together with both *in situ* production and *ex situ* input of the relatively slow oxidizing I^-—transported from underlying anoxic waters characterized by quantitative IO_3^- reduction—results in steep $[IO_3^-]$ gradients (Farrenkopf and Luther III, 2002; Lu et al., 2016; Rue et al., 1997; Wong and Brewer, 1977). Modern seawater non-zero $[IO_3^-]$ values of <250 nM are almost exclusively found in such settings (Fig. 1; Chance et al., 2014; Lu et al., 2016). This low range of seawater $[IO_3^-]$ would be recorded as I/(Ca+Mg) ratios of <~2.6 μmol/mol in carbonate, as observed in both laboratory calcite-precipitation experiments (Lu et al., 2010) and direct measurements of modern carbonate from low oxygen settings (Glock et al., 2014; Lu et al., 2016). Analogous to the oxyclines of modern OMZs and anoxic basins, ancient carbonate with non-zero I/(Ca+Mg) of less than ~2.6 μmol/mol are interpreted to reflect precipitation within waters with local O_2 levels above those necessary to sustain IO_3^- accumulation, but which are also characterized by or in frequent exchange with waters hosting active IO_3^- reduction (Lu et al., 2016).

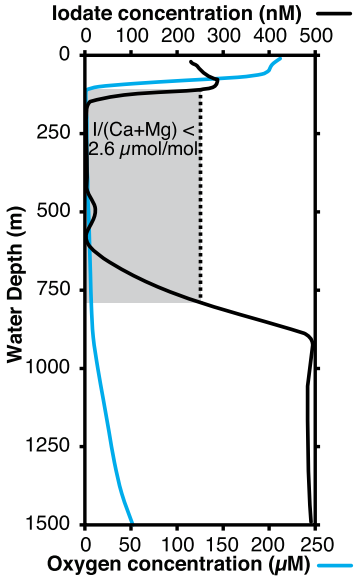

Fig. 1. Water column dissolved $[IO_3^-]$ and $[O_2]$ from a vertical transect through the Peruvian OMZ (Rue et al., 1997). The vertical dashed line highlights the range of $[IO_3^-]$ (<250 nM) that is nearly exclusively observed in settings within or below the oxycline of marine anoxic basins and OMZs (Lu et al., 2016). The shaded box refers to the portion of the profile where corresponding I/(Ca+Mg) ratios are anticipated to be <2.6 μmol/mol (Glock et al., 2014; Lu et al., 2016), which is further discussed in the main text.

Importantly, diagenetic effects on I/(Ca+Mg) ratios have not been examined in previous studies. Given that diagenetic carbonate minerals form most often from anoxic pore fluids (Loyd et al., 2012; McClain et al., 1992; Schrag et al., 2013) marked by IO_3^- reduction, carbonate phases are expected to be particularly sensitive to diagenetic iodine loss. Carbonates of the Proterozoic Eon host the largest positive and negative $\delta^{13}C_{carb}$ excursions in Earth history—the Paleoproterozoic Lomagundi and Ediacaran Shuram anomalies, respectively. Although differing in direction, both have been interpreted as large-scale Proterozoic oxidation events bracketing the overall mid-Proterozoic low oxygen atmosphere (e.g., Fike et al., 2006; Lyons et al., 2014). However, these records are at best only indirect measures of redox conditions in the surface ocean, and their relationships to the broader workings of the carbon cycle as manifested in marine water column signals can be lost or overprinted during diagenesis by pore fluid chemistry (Schrag et al., 2013; Swart and Kennedy, 2012). If the effects of diagenesis on I/(Ca+Mg) are understood, examination of I/(Ca+Mg) through Proterozoic carbon isotope excursions may provide a means of testing whether these records represent pore fluid or water column chemistry.

Table 1
Approximate ages and number of samples for Proterozoic geologic units measured for I/(Ca+Mg) ratios in this study. References to ages and lithological descriptions can be found in the supplementary materials.

Geologic unit	Approximate age (billions of years)	*n*
Wooly Dolomite, Australia	2.03	11
Snare Group, Canada	1.97	4
Taltheilei Formation, Canada	1.88	14
Duck Creek Formation, Australia	1.80	22
Paradise Creek Formation, Australia	1.65	10
Helena Formation, USA	1.45	9
Tieling Formation, China	1.44	45
Kaltasy Formation, Russia	1.43	12
Dismal Lakes Group, Canada	1.30	16
Mescal Formation, USA	1.26	4
Angmaat Formation, Canada	1.15	17
Atar and El Mreiti groups, Mauritania	1.10	17
Sukhaya Tunguska Formation, Russia	1.04	7
Shaler Group, Canada	0.85	17
Akademikerbeen Group, Svalbard; Limestone-Dolomite Series, Greenland	0.83	36
Beck Springs Dolomite, USA	0.75	20
Khufai Formation, Sultanate of Oman	0.58	122
Johnnie Formation, USA	0.58	30
Clemente Formation, Mexico	0.58	31
Doushantuo Formation, China (Siduping)	0.64–0.58	74

Here we provide the most comprehensive record of Proterozoic surface ocean redox to date, specifically tracking temporal marine IO_3^- availability through a compilation of I/(Ca+Mg) ratios from mostly shallow-marine carbonate rocks (limestones and dolostones). This data set includes carbonates capturing the Shuram $\delta^{13}C_{carb}$ excursion. We also provide the first constraints on iodine proxy response to diagenetic alteration of recent carbonates. Through comparisons of dissolved iodine cycling in modern low-oxygen versus well-oxygenated marine waters, I/(Ca+Mg) records from pristine modern carbonates from both redox end members, and diagenetic carbonates from Neogene–Quaternary settings, we suggest that oxygenation in the surface ocean following the GOE was consistent with that necessary to sustain simple eukaryotic life. At the same time, the low I/(Ca+Mg) ratios typical of the mid-Proterozoic reflect carbonate precipitation in waters with overall low and unstable oxygen levels in close spatial proximity to anoxic waters. In addition, we provide evidence against diagenesis as a driver of the Shuram excursion.

2. Materials

We measured I/(Ca+Mg) ratios of carbonate rocks ($n = 518$) from 20 sedimentary successions spanning the late Paleoproterozoic to late Neoproterozoic (Table 1) and combined these results with previously published carbonate iodine data (Glock et al., 2014; Hardisty et al., 2014; Loope et al., 2013; Lu et al., 2016, 2010; Owens et al., 2017; Zhou et al., 2014, 2015). Details regarding age, stratigraphy, and complementary geochemistry for the individual sections are included in the Supplementary Materials. This data set also includes new results from four previously studied carbonate sections that capture the Ediacaran Shuram negative $\delta^{13}C_{carb}$ anomaly: the Khufai Formation of the Sultanate of Oman (Osburn et al., 2015); the Doushantuo Formation of South China; the Johnnie Formation of Death Valley, USA; and the Clemente Formation of northern Mexico (Loyd et al., 2013). For this and the previously published Precambrian iodine data (Hardisty et al., 2014), emphasis was placed on carbonate successions with independent sedimentological evidence for shallow-marine deposition and units with clear indications of secondary alteration, such as veins and metamorphism above greenschist grade, were avoided.

Table 2
Approximate ages and number of samples for Neogene–Quaternary geologic units measured for I/(Ca+Mg) ratios in this study. Also shown are the diagenetic conditions affecting mineralogy at each study site. The relevant previous publications providing lithological, geochemical, and diagenetic constraints are provided in the Supplementary Materials and in some cases in the main text. Supplementary Fig. 1 contains a map of the sampling localities.

Age	Location	Diagenetic setting	*n*
Modern	Little Darby and Lee Stocking Islands, Bahamas	initial deposition	57
Pleistocene	Key Largo Limestone, South Florida	initial deposition, meteoric	30
Neogene–Quaternary	Clino, Bahamas	meteoric, marine burial, dolomitization	151
Neogene–Quaternary	Unda, Bahamas	dolomitization	49
Miocene	Monterey Formation, Central California	authigenic dolomite concretions	24

To evaluate the effects of diagenetic mineral transformations on I/(Ca+Mg) ratios, we include a series of Neogene–Quaternary case studies to provide a comprehensive view of initial iodine precipitation and subsequent modification as a function of varying primary carbonate mineralogy, carbonate burial history, and related diagenetic pathways—specifically, meteoric diagenesis, marine burial diagenesis, and dolomitization. The case studies are outlined below (along with citations to detailed previous studies of the same localities or samples), in Table 2, and in the Supplemental Materials:

(1) **Short (ca. <16 cm) bank-top cores from the modern Great Bahama Bank, or GBB** (Romaniello et al., 2013; Zhang et al., 2017). These samples capture initial iodine deposition with primary carbonates from a range of shallow settings and primary mineralogies near Little Darby and Lee Stocking islands (Table 3; Supplementary Figs. 1 and 2).
(2) Montastrea annularis **coral heads from the Pleistocene Key Largo Limestone, South Florida**. This sample set includes aragonite-to-low-Mg calcite (LMC) transitions driven by subaerial exposure and subsequent diagenesis in meteoric pore waters. Post-depositional organic matter remineralization during aragonite-to-calcite neomorphism has resulted in negative $\delta^{13}C_{carb}$ values in some of the LMC samples (Gill et al., 2008).
(3) **The Neogene–Quaternary Clino and Unda cores, Great Bahama Bank.** These cores were drilled ~8 km apart along the western edge of the Great Bahama Bank (Supplementary Fig. 1). The Clino core contains a negative $\delta^{13}C_{carb}$ excursion in the upper portion reflecting multiple periods of subaerial exposure and subsequent aragonite-to-calcite neomorphism in meteoric pore fluids (still ongoing at the top of the core), along with intervals with aragonite-to-calcite neomorphism occurring exclusively in marine pore fluids and minor dolomite, which were all sampled in detail (Melim et al., 1995; Swart and Melim, 2000; Swart and Kennedy, 2012). The Unda and Clino cores have similar depositional histories; however, for the purposes of this study, we did not sample the Unda core in the same stratigraphic detail as the Clino core. For the Unda core, we specifically sampled two intervals of extensive dolomite that formed in exchange with marine pore fluids (Swart and Melim, 2000).
(4) **Dolomite concretions of the Miocene Monterey Formation, California.** These samples represent dolomite derived mainly from alkalinity production and authigenic carbonate precipitation during remineralization of organic carbon in marine pore fluids, in contrast to recrystallization of carbonate precursors (Loyd et al., 2013).

Table 3
Coordinates, water depth, key depositional features, and mineralogy for cores from near Little Darby and Lee Stocking Islands, Bahamas. Mineralogy is shown in wt.% of high-Mg calcite (HMC). None of the cores contained dolomite and only minor calcite was found in the cores, with HMC+aragonite >93.52 wt.% in all cases, meaning that the sediments mostly consist of aragonite. The detailed mineralogy, $\delta^{13}C_{carb}$, $\delta^{18}O_{carb}$, and I/(Ca+Mg) for each sample can be found in Supplementary Table 1. Also shown is the I/(Ca+Mg) value for uppermost sediment sample and the range for all depths from each short core. Supplementary Fig. 1 contains a map of the sampling localities and Supplementary Fig. 2 shows vertical profiles of I/(Ca+Mg), $\delta^{13}C_{carb}$, and wt.% aragonite for each of the cores.

Core	Coordinates	Water depth (m)	Key features	HMC (wt.%)	I/(Ca+Mg) (μmol/mol)	
					Surface	Range
C1	23°51′24.59″N 76°13′30.85″W	<1	intertidal	6.6–23.0	10.2	8.1–10.2
C3	23°51′24.68″N 76°13′33.25″W	<5	subtidal/*Thalassia testudinum* bed	15.2–25.6	7.6	6.7–7.6
C4, C6	23°46′11.21″N 76° 6′48.92″W	<10	subtidal/former ooid shoal/peloid rich/*Thalassia testudinum* bed	13.7–31.3; 8.1–26.5	10.0; 9.4	8.4–10.8; 7.7–9.4
C5	23°45′57.18″N 76°8′3.00″W	<10	subtidal/active ooid shoal/ooid aggregates or grapestones	4.7–9.3	11.6	6.0–11.6
C7	23°46′10.78″N 76°6′51.48″W	<10	subtidal/active ooid shoal/ooid aggregates or grapestones	4.3–10.3	7.2	6.7–7.5
C8	23°51′21.55″N 76°13′33.52″W	<2	subtidal/active ooid shoal/ooid aggregates or grapestones	8.8–24.1	8.2	6.3–8.2

3. Methods

Iodine-to-calcium-magnesium ratios and magnesium-to-calcium ratios were measured at Syracuse University using a Bruker M90 quadrupole inductively-coupled-plasma mass spectrometer (ICP-MS) and at the University of California, Riverside, using a Agilent 7900c ICP-MS, according to standard methods (Hardisty et al., 2014; Lu et al., 2010, 2016; Zhou et al., 2014, 2015). All samples from the Clino and Unda cores and the Monterey and Tieling formations were measured at UC Riverside and the remainder at Syracuse University. Approximately 3–5 mg of powdered carbonate was used for each analysis. Samples were sonicated in 1 mL DI water that was then centrifuged and decanted. Following this, 3% HNO_3 was added to each sample allowing for complete dissolution of all carbonate, and these were similarly sonicated for ~10 minutes and centrifuged. The supernatant was diluted in a matrix with combinations of nitric acid and an iodine-stabilizing solution (tertiary amine or tetramethyl ammonium hydroxide) to obtain Ca concentrations of approximately 50 ppm. Calibration standards were made fresh each day from powdered potassium iodate in a similar matrix with the addition of 50 ppm Ca. The coral standard JCP-1 was analyzed intermittently with average values at Syracuse University and UC Riverside that were identical within error.

The mineralogical determinations for the Clino and Unda cores, Monterey, Key Largo, and Bahamas Bank top cores were performed at the University of Miami using a Panalytical X-Pert Pro via a method published previously (Melim et al., 1995). The associated error is ±2 wt.%. Carbon and oxygen isotope values for the Johnnie Formation, the Clino and Unda cores, and portions of the GBB short cores were measured at the University of California, Riverside, using a GasBench II interface coupled, via continuous flow, to a Delta V Thermo Advantage IRMS (Isotope Ratio Mass Spectrometer). Carbon and oxygen isotope values for the C1, C4, C6, and C7 Bahamas Bank top cores were analyzed at The Center for Stable Isotope Biogeochemistry at UC, Berkeley, using a MultiCarb system connected with a GV IsoPrime mass spectrometer in dual inlet mode. Carbon and oxygen isotopes for the Doushantuo Formation were measured at the University of Nevada, Las Vegas, using a Kiel IV carbonate device connected to a Finnigan Delta V Plus mass spectrometer in dual inlet mode. All values are presented in the standard delta notation as per mil (‰) deviation from Vienna Pee Dee Belemnite (V-PDB), with replicate standard analyses yielding standard deviations typically better than 0.10‰ for carbon and oxygen isotopes.

4. Results

The highest I/(Ca+Mg) values in our Neogene–Quaternary samples, ranging from 6.0–11.6 μmol/mol, are found in predominantly aragonite and HMC samples from bank-top cores from the well-oxygenated GBB (Table 3). The Key Largo coral heads contain I/(Ca+Mg) values that show little change across the meteoric fluid-driven aragonite-to-calcite mineralogy transition, with only KL-11 containing samples with decreased iodine contents in some, but not all, LMC-dominated samples (Fig. 2). For cores Clino and Unda, the carbon and oxygen isotopic and mineralogical trends and values within specific intervals are generally consistent with that of previous work of different samples from the same core (e.g., Melim et al., 1995; Swart and Melim, 2000; Swart and Kennedy, 2012), including the negative $\delta^{13}C_{carb}$ excursion characterizing the meteoric zone in the Clino core (Fig. 3). The Clino core contains I/(Ca+Mg) ranging from below detection to 5.71 μmol/mol. The highest I/(Ca+Mg) values overlap with intervals containing relatively higher aragonite content, with most LMC- and dolomite-dominated intervals generally containing relatively lower I/(Ca+Mg) ratios (Fig. 4). The Unda and Monterey samples have I/(Ca+Mg) values ranging from below detection to 0.46 and 1.01 μmol/mol, respectively (Fig. 4). Of the samples containing greater than 20 wt.% dolomite, I/(Ca+Mg) ratios are <0.46 and 0.40 μmol/mol for the Monterey Formation and the Unda core, respectively, with most values below detection.

Our Proterozoic samples contain both dolomite and limestone (Fig. 5), and iodine is present in some of the samples from nearly all the units evaluated (Fig. 6). Proterozoic I/(Ca+Mg) ratios from carbonates older than the late Ediacaran Shuram anomaly are ≤2.8 μmol/mol and are often much less—notably within the range observed in primary carbonate from modern low-oxygen settings (yellow squares, Fig. 6). There is a drop in maximum I/(Ca+Mg) to ≤0.8 μmol/mol around ~2.0 Ga, following the Lomagundi positive carbon isotope excursion (LE; ~2.2–2.1 Ga). In the following interval, from 2.0 to 1.0 Ga, maximum values of ≤0.8 μmol/mol are found in 13 of the 14 studied units with the only exception being the Tieling Formation of North China, where maximum I/(Ca+Mg) ratios are similar to those characterizing the LE and early Neoproterozoic (Fig. 6). Starting at roughly 1.0 Ga, maximum values are more frequently elevated relative to the mid-Proterozoic. Lastly, all four of our Ediacaran, Shuram-age sections show a marked increase in I/(Ca+Mg) in phase with the dramatic decrease in $\delta^{13}C_{carb}$ (Fig. 7).

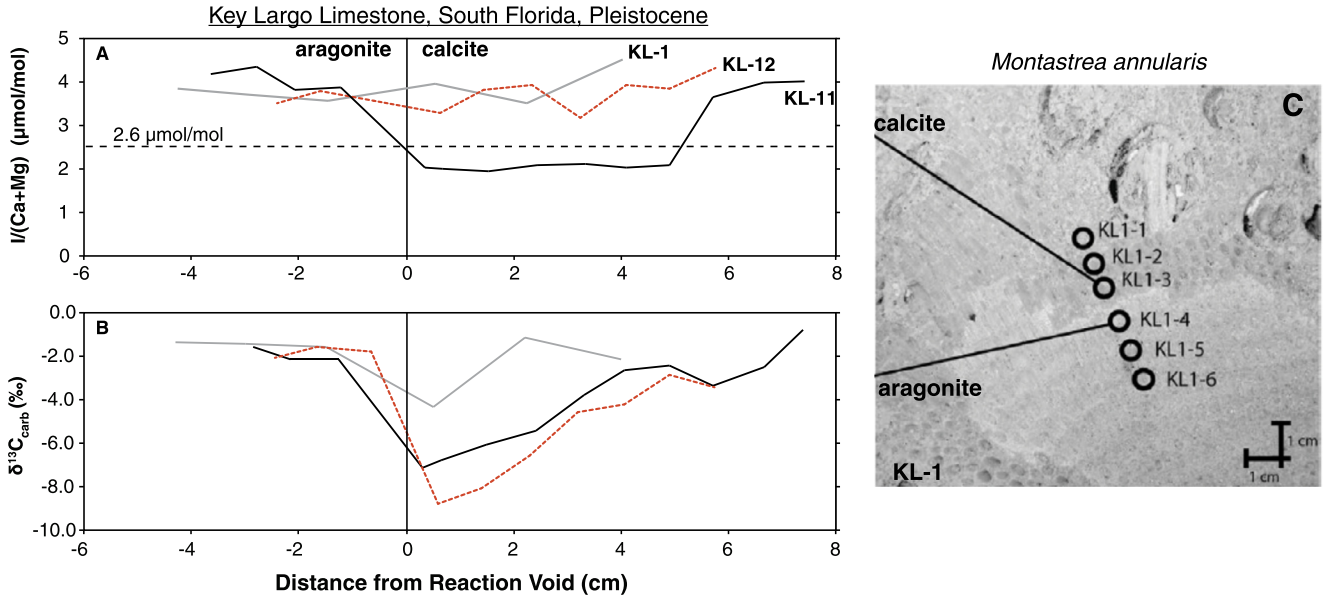

Fig. 2. (a) I/(Ca+Mg) and (b) $\delta^{13}C_{carb}$ for transects through three aragonite-dominated to calcite-dominated portions of (c) *Montastrea annularis* coral heads of the Pleistocene Key Largo Limestone of South Florida. The samples and transects are exactly the same as those used in Gill et al. (2008). The horizontal dashed line at 2.6 µmol/mol (part a) represents the I/(Ca+Mg) ratio range found in calcitic forams from low oxygen water column settings (Glock et al., 2014; Lu et al., 2016). A picture of the KL-1 coral head and drilled transect is shown in part c as an example, with the circles representing discrete sampling locations. The transect is drilled at centimeter intervals across a mineralogical transition from aragonite to calcite driven by subaerial exposure and diagenesis in meteoric pore fluids. The aragonite can be discerned by the lighter color and the calcite by the darker color, with the reaction void occurring between KL1-3 and KL1-4. Scale bar in bottom right hand corner is 1 cm.

5. Discussion

5.1. Iodine behavior in response to Neogene–Quaternary carbonate diagenesis

No previous study has measured carbonate iodine contents within an independently established framework of well-constrained diagenetic alteration. Interpretation of iodine contents of water column-derived calcitic foraminifera is obviously ideal; however, this is not always possible in ancient samples. Multiple previous studies have instead measured bulk iodine in ancient carbonate (Hardisty et al., 2014; Loope et al., 2013; Zhou et al., 2015; Owens et al., 2017). Below we provide a context for interpreting our Proterozoic bulk carbonate data through a process-oriented perspective in Neogene–Quaternary carbonate of the Bahamas and Monterey Formation that progresses from modern carbonate precipitation to deposition, burial, and subsequent variable styles of diagenetic mineral transformation. With the exception of the Monterey Formation, the waters that hosted primary carbonate precipitation are constrained to have been well oxygenated, which implies that presently low and highly variable I/(Ca+Mg) ratios do not record shifts in the IO_3^- content of the local waters of deposition. Instead, low I/(Ca+Mg) values or variations likely track secondary processes related to depositional setting, mineralogy, and related diagenetic overprinting of primary values.

The highest I/(Ca+Mg) ratios in our Neogene–Quaternary sample set come from the GBB bank-top cores (Table 3), which is the least altered sample set of this study and representative of the carbonate iodine signature of initial deposition. The range in I/(Ca+Mg) values from bulk aragonite-HMC in all the GBB bank-top core samples (6.0–11.6 µmol/mol; Table 3) is higher than that found in LMC foraminifera, which in previous studies of well-oxygenated settings spans from 4–7 µmol/mol (Lu et al., 2016). None of our I/(Ca+Mg) profiles from any of the seven GBB short cores increases with depth (Table 3; Supplementary Fig. 2), indicating that the elevated I/(Ca+Mg) values are unrelated to post-burial processes. Uncertainties surrounding partition coefficients for HMC and aragonite relative to that of calcite and potential vital effects associated with uncharacterized skeletal debris may lead to errors in the estimated IO_3^- content of ambient waters from variable carbonate mineralogies. Until the partition coefficients of iodine for individual carbonate mineralogies are resolved, caution should be taken in comparing absolute I/(Ca+Mg) ratios between samples of mixed or unknown carbonate mineralogy. For example, if we apply the partition coefficients from laboratory LMC precipitation experiments (Lu et al., 2010; Zhou et al., 2014) to the I/(Ca+Mg) ratios from our aragonite- and HMC-dominated GBB carbonate, we predict local marine IO_3^- abundance from ~600 nM to approaching 1 µM, which is not consistent with the typical range observed in marine, surface waters (roughly 300 to 450 nM; Chance et al., 2014). However, the wide and elevated range in I/(Ca+Mg) from the GBB is not easily attributed to any one factor, as the GBB I/(Ca+Mg) ratios differ even between adjacent oolitic shoals of similar composition and show no clear co-variation with mineralogy, $\delta^{13}C_{carb}$, or modern depositional setting (Table 3; Supplementary Fig. 2). Regardless, our observations are consistent with previous works indicating that the I/(Ca+Mg) ratios of primary carbonate minerals precipitated from well-oxygenated seawater do not overlap with the 0–2.6 µmol/mol values observed for calcitic foraminifera living within low-oxygen settings (Glock et al., 2014; Lu et al., 2016).

The Key Largo coral heads provide a case study specific to initial aragonite precipitation and post-depositional meteoric aragonite-to-calcite neomorphism during subaerial carbonate exposure (Gill et al., 2008). In this case, the I/(Ca+Mg) ratios of primary aragonite fall within the range reported for LMC foraminifera from well-oxygenated settings (Fig. 2). Previous work from these same samples has shown that lower dissolved elemental abundances (e.g., S, Sr) in fresh (meteoric) waters versus seawater, which to a lesser extent is also true of iodine (Fehn, 2012), lead to decreases in their concentrations in diagenetic LMC relative to primary aragonite (Gill et al., 2008). Opposite of this expectation, however, the primary I/(Ca+Mg) ratios generally change little across the aragonite-to-calcite transitions of our samples. The only exception is a LMC interval directly at the reaction front of KL-11 that contains lower I/(Ca+Mg) relative to the primary aragonite (Fig. 2),

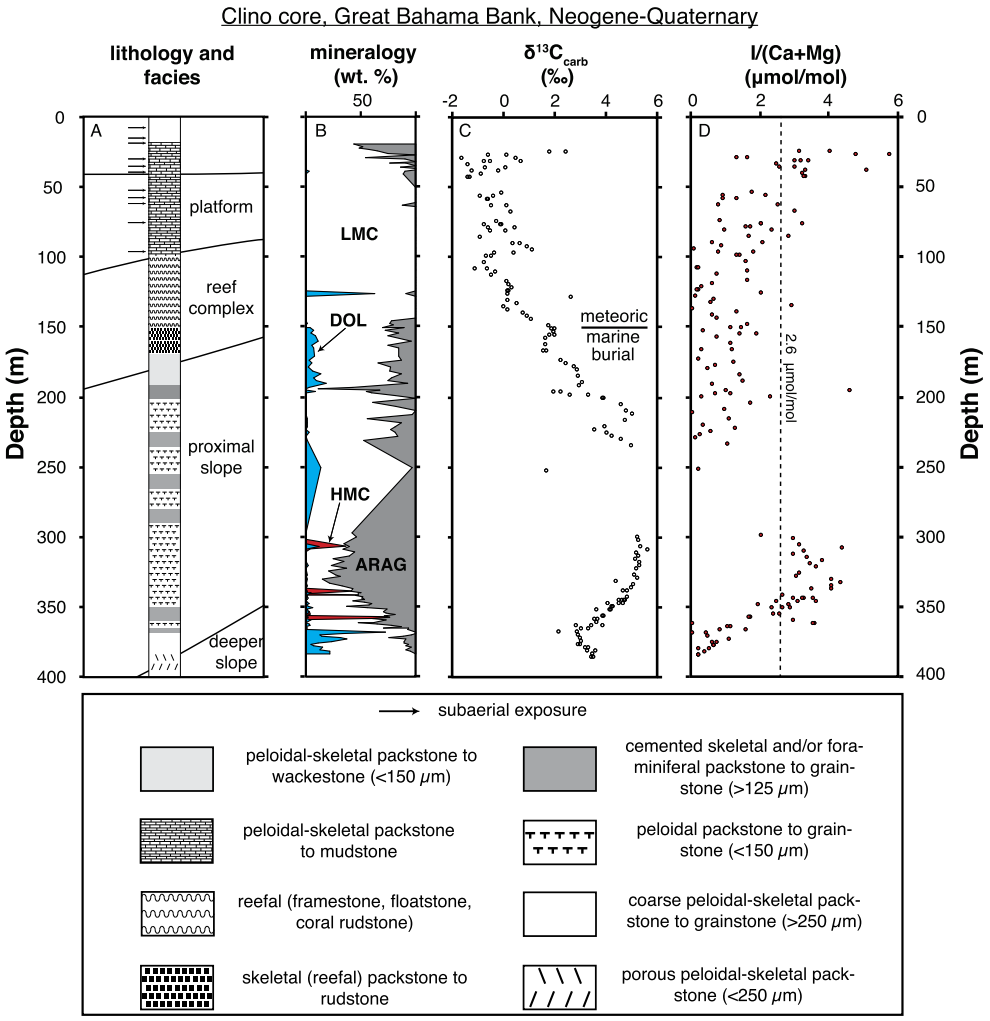

Fig. 3. The (a) facies and lithology (horizontal and slanted lines represent ramp paleo geometry; Swart and Melim, 2000), (b) carbonate mineralogy (aragonite–dark grey; HMC–red, LMC–white; dolomite–blue), (c) $\delta^{13}C_{carb}$, and (d) I/(Ca+Mg) ratios for the Clino core of the Great Bahama Bank. Lithological descriptions come from Kenter et al. (2001) and Manfrino and Ginsburg (2001). The vertical dashed line at 2.6 μmol/mol represents the I/(Ca+Mg) ratio range found in calcitic forams from low oxygen water column settings (Glock et al., 2014; Lu et al., 2016). (For interpretation of the references to color in this figure legend, the reader is referred to the web version of this article.)

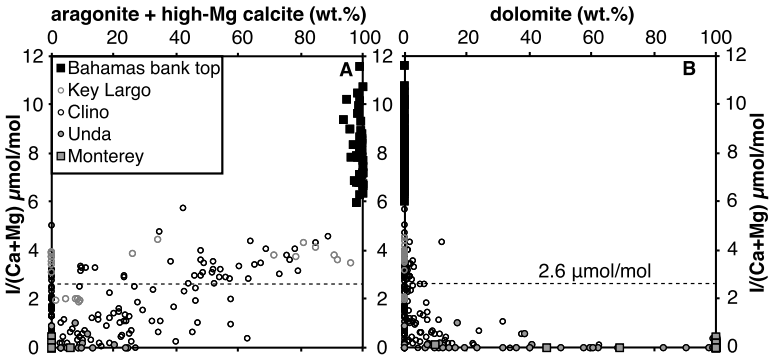

Fig. 4. The composition of (a) primary aragonite and high-Mg calcite and (b) diagenetic dolomite relative to I/(Ca+Mg) ratios for the diagenetic sample set described in the main text and labeled in the legend. The horizontal dashed line is at an I/(Ca+Mg) of 2.6 μmol/mol, the threshold, which, as discussed in the text, is characteristic of reducing marine setting (Glock et al., 2014; Lu et al., 2016).

but there are no discernable differences between these and other LMC samples with relatively elevated I/(Ca+Mg). The maintenance of high, primary I/(Ca+Mg) ratios during meteoric diagenesis in the Key Largo samples may represent a special case where oxic diagenetic conditions allowed for the iodine content of the primary aragonite to (at least temporarily) buffer iodine contents of the diagenetic LMC. Sulfate reduction is known to partially promote aragonite-to-calcite neomorphism during meteoric diagenesis in the Bahamas (McClain et al., 1992)—conditions where iodine would be present primarily as I^-. However, the $\delta^{34}S$ values of carbonate-associated sulfate (CAS) in both our original aragonite and secondary LMC Key Largo samples are similar to those of Pleistocene/modern seawater sulfate (Gill et al., 2008), arguing against substantial sulfate reduction during meteoric diagenesis. Nonethe-